Optimization of Phase-Engineered a-Si:H-Based Multijunction Solar Cells

Principal Investigators:
Christopher R. Wronski and Robert W. Collins

Participants:
Joshua Pearce, Jingdong Deng, Vasilios Vlahos,
Gelio M. Ferreira, and Chi Chen

Center for Thin Film Devices

The Pennsylvania State University
University Park, PA 16802

Quarterly Technical Status Report
August 2003 – October 2003

Subcontract No. NDJ-1-30630-01

NREL Technical Monitor: Dr. Bolko von Roedern

Executive Summary

Task 1: Materials Research and Device Development:
Optimization of rf and vhf PECVD Materials for High Rate i-layers of Si:H Solar Cells Based on the Deposition Phase Diagram

(1) Under H_2 deficient dilution conditions, vhf (60 MHz) PECVD provides significant advantages over rf (13.56 MHz) PECVD in the fabrication of higher quality a-Si:H at high rates. Under optimum conditions, however, with the H_2-dilution ratio set just below the a→(a+μc) transition for the desired film thickness, vhf PECVD provides no significant advantage over rf PECVD when identical high deposition rates are compared.

(2) In a high plasma power, high pressure (3 Torr) rf PECVD process for a-Si:H film growth, the amorphous phase roughening transition thickness remains above 1000 Å just below the a→(a+μc) boundary where the rate is 6.5 Å /s. This transition thickness is a factor of two higher than that observed under low pressure deposition conditions with almost a factor of two lower deposition rate for the a-Si:H. As a result, we suggest that the high power, high pressure conditions may give rise to reasonable device performance at rates > 6 Å/s, without resorting to unconventional deposition methods.

Task 2: Process Improvement directed by Real Time Diagnostics:
Optimization of rf and vhf PECVD Materials for High Rate i-layers of Si:H Solar Cells Based on the Deposition Phase Diagram

(1) Three manifestations of enhanced precursor surface diffusion are evident with increasing H_2-dilution ratio R under all conditions of a-Si:H deposition explored here: (i) increased surface smoothening (both rate and amplitude) associated with the coalescence of initial nuclei in the first 100 Å of deposition; (ii) reduced surface roughness layer thickness at the stable surface value; and (iii) increased surface stability as measured by the thickness of the a→a roughening transition. The presence of all three effects provide clear signatures of improved device-quality materials based on the monolayer level processes detected at the film surface

(2) The similarities of the phase diagrams for both rf and vhf PECVD of Si:H on R=0 a-Si:H substrate films demonstrate that the two-step optimization procedure developed

for the rf PECVD protocrystalline i-layers of a-Si:H-based p-i-n and n-i-p cells would also apply for vhf PECVD i-layers as well.

Task 3: Device Loss Mechanisms

(1) Studies of the device loss mechanisms in a-Si:H solar cells have been continued during this quarter and the potential of the dark J_D-V characteristic to serve as a sensitive probe of the cells has been further established using p-i-n cell structures with R=0 and R=10 i-layers of different thickness. Results have been obtained for the current voltage regimes over which bulk recombination dominates the characteristics. Excellent agreement is obtained over five orders of magnitude in currents between the derived J_D-V characteristics in which the recombination at the p/i interfaces is taken into account and those in cell structures with optimized p/i interface regions. Establishing the voltage regimes over which the bulk contribution dominates now allows the remaining J_D-V characteristics to be investigated in terms of p/i interface recombination and the limitations imposed on the carrier injection by the potential barriers in the i-layers adjacent to the p and n contacts. This is being carried out by characterizing the differential diode quality factors, $n(V)=[kT/q]^{-1}[d(\ln J_D)/dV]^{-1}$, in cells having significant differences in p/i interface recombination obtained with different cell structures. The contributions of these two components to fill factors and open circuit voltages under 1-sun illumination can then be evaluated.

(2) In addition, the regimes corresponding to bulk recombination are being utilized in investigating the gap states of the R=0 and R=10 i-layers both in the annealed state as well as during the introduction of light induced defects. The results for these i-layers show significant differences and are being compared with the corresponding results from studies of films in which large differences in the evolution of two types of defect states has also been found[1]. The results obtained for the evolution of SWE defects by photo-generation of carriers as well as carrier injection, are being correlated with differential sub-gap absorption, $d(\alpha(E))/dE$, as well as results for the evolution of D^o states as measured by ESR at the University of Utah on the same intrinsic materials.

[1] J. M. Pearce, J. Deng, R. W. Collins, and C. R. Wronski, *Appl. Phys. Lett*., 2003 (in press)

Report Including: Task 1: Materials Research and Device Development

Task 2: Process Improvement directed by Real Time Diagnostics

Evaluation of Materials and Processes for High Rate Growth of Si:H by vhf PECVD

Overview

In order to increase deposition rate and throughput for Si:H-based solar cell production by plasma-enhanced chemical vapor deposition (PECVD), and therefore to reduce costs, very high frequency (vhf) plasma excitation, typically within the range from 50 to 100 MHz, has been widely considered as an alternative to conventional rf excitation at 13.56 MHz. The vhf frequencies have been proposed to be more effective in dissociating the $SiH_4 + H_2$ mixtures, thus providing higher rate fabrication of amorphous and microcrystalline Si:H near the $a \rightarrow (a+\mu c)$ and $(a+\mu c) \rightarrow \mu c$ deposition phase boundaries (see below).

The goal of our recently completed investigations has been to explore the effects of plasma excitation frequency on Si:H PECVD, comparing real time spectroscopic ellipsometry (RTSE) results for the microstructural evolution of f = 13.56 MHz (rf) and f = 60 MHz (vhf) Si:H materials. The information deduced from RTSE can be summarized succinctly using deposition phase diagrams wherein one or more of the deposition phase boundaries are plotted in the plane of the H_2-dilution ratio $R=[H_2]/[SiH_4]$ (abscissa) and the accumulated bulk layer thickness d_b (ordinate). R is the parameter exerting the strongest influence on the Si:H phase evolution and so is the most natural parameter to be used as the abscissa of this diagram.

The phase diagrams that we have developed include three different microstructural transitions as observed with the highest sensitivity through the surface roughness evolution.

(i) The *amorphous roughening transition [denoted a→a]* provides insights into the device suitability of a-Si:H materials. In fact, the highest device-quality materials exhibit the most stable surfaces and thus the largest a→a roughening transition thickness.

(ii) The *amorphous–to–(mixed-phase-microcrystalline) (a+μc) roughening transition [denoted a→(a+μc)]* identifies the optimum R value for a-Si:H deposition under otherwise fixed conditions. This optimum generally occurs at the maximum R just before the a→(a+μc) transition is crossed for the given thickness. Here the largest a→a roughening transition thickness occurs.

(iii) The (*mixed-phase-microcrystalline)–to–(single-phase-microcrystalline) smoothening transition [denoted (a+μc)→μc]* appears to identify the optimum conditions for the fabrication of μc-Si:H materials. These conditions occur at the lowest R value possible while ensuring single-phase μc-Si:H deposition.

In summary, the deposition phase diagrams provide insights into the comparative device suitability of Si:H materials. The deposition processes studied here using both rf and vhf plasma excitation for an in-depth frequency comparison include:

(1) minimum plasma power (0.08 W/cm^2) and low gas pressures (< 0.5 Torr), yielding rates of **0.5 - 1.5 Å/s** just before the a→(a+μc) boundary (R=10) for a thick film (4000 Å),

(2) elevated plasma power (0.34-0.53 W/cm^2) and high pressure (4 Torr), yielding rates of **3.2 - 3.4 Å/s** just before the a→(a+μc) boundary (R=60) for a thick film (4000 Å),

(3) elevated plasma power (0.53-0.72 W/cm^2) and high pressure (3 Torr), yielding **6.5 Å/s** just before the a→(a+μc) boundary (R=60) for a thick film (4000 Å).

Low Power and Pressure Si:H Depositions: Crystalline Si Wafer Substrates

Figure 1 shows deposition rates as a function of R for Si:H films prepared by rf (13.56 MHz) and vhf (60 MHz) PECVD at the minimum plasma power (0.08 W/cm^2)

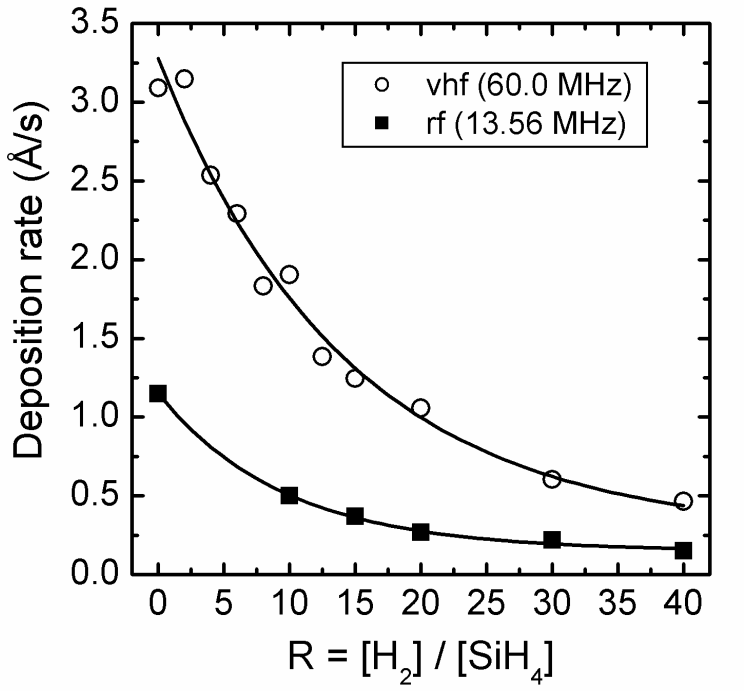

Figure 1: Comparison of the deposition rates for rf (13.56 MHz) and vhf (60 MHz) PECVD as a function of R under low power (0.08 W/cm^2) and low pressure (< 0.5 Torr) conditions.

and low pressures (< 0.5 Torr, total) [process (1)]. For both deposition series in Fig. 1, the films were prepared in a PECVD reactor having a parallel-plate electrode configuration with an electrode spacing of 1.9 cm, and the substrate temperature was fixed at 200°C. The partial pressure of SiH_4 was fixed at ~0.05 Torr, while the total $[SiH_4]+[H_2]$ pressure increased from 0.07 to 0.5 Torr with the increase in R.

Figures 2 and 3 depict the microstructural evolution, i.e., the surface roughness layer thickness versus the bulk layer thickness as deduced by RTSE for the vhf PECVD Si:H films of this series prepared at different hydrogen dilution levels $R=[H_2]/[SiH_4]$ on smooth, native oxide-covered c-Si substrates. The series versus R for $0 \leq R \leq 8$ in Fig. 2 depicts films that remain amorphous throughout growth and thus exhibit the weak a→a roughening transitions, whereas the films in Fig. 3 for R>10 exhibit abrupt a→(a+μc) roughening transitions as well as abrupt (a+μc)→μc smoothening transitions during growth. (Note the difference in the vertical roughness scales between the two figures.)

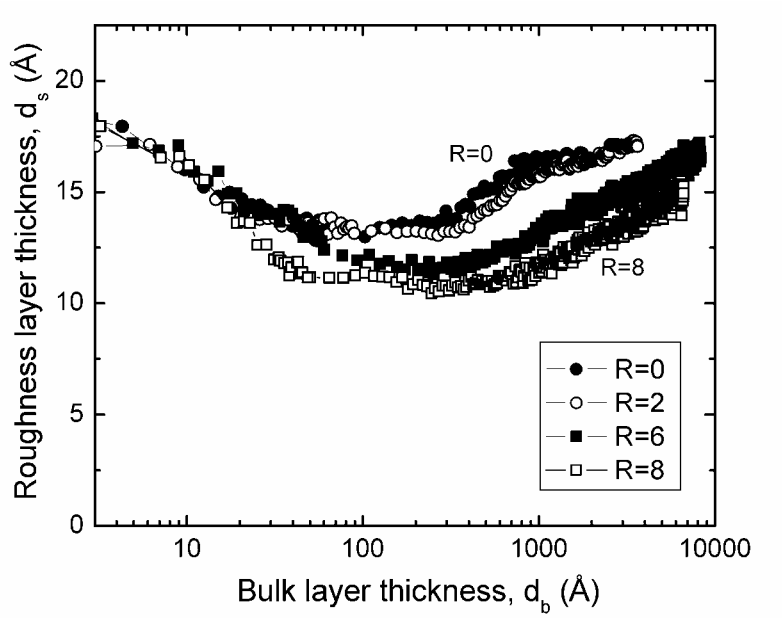

Figure 2: Surface roughness layer thickness (d_s) versus bulk layer thickness (d_b) for growth of single-phase amorphous Si:H films by vhf (60.0 MHz) PECVD using H_2-dilution levels of R=0, 2, 6, and 8 in the low power (0.08 mW/cm^2) and low pressure (< 0.5 Torr) process on smooth (nat. oxide)/c-Si substrates.

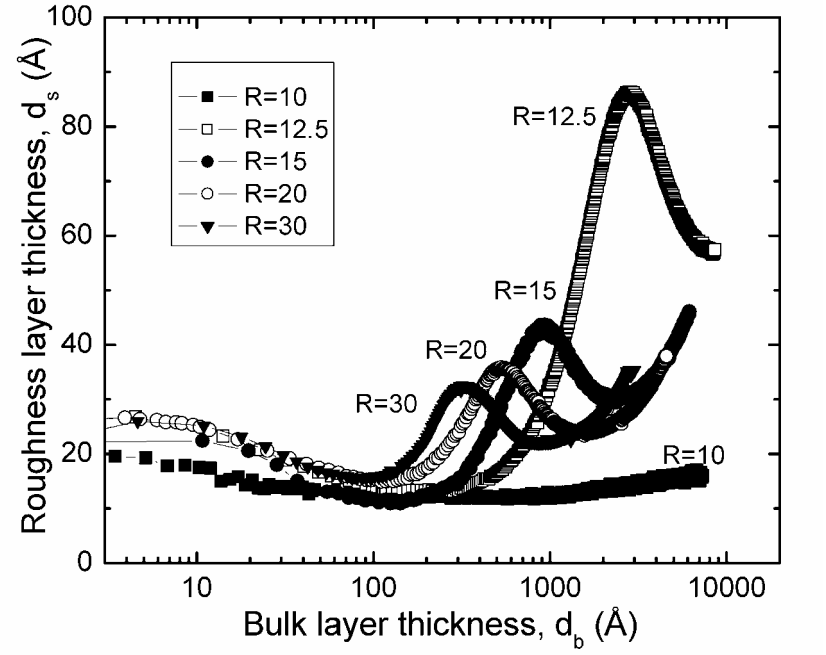

Figure 3: Surface roughness layer thickness (d_s) versus bulk layer thickness (d_b) for growth of Si:H films by vhf (60.0 MHz) PECVD using H_2-dilution levels of R=10, 12.5, 15, 20, and 30 in the low power (0.08 mW/cm^2) and low pressure (< 0.5 Torr) process on smooth (nat. oxide)/c-Si substrates. All films except the one with R=10 exhibit a→(a+μc) roughening as well as (a+μc)→μc smoothening transitions during growth.

Figure 4 shows the superimposed phase diagrams for this series of vhf (60 MHz) PECVD Si:H films along with the corresponding data for the rf (13.56 MHz) PECVD Si:H films also obtained at minimum power and low pressure. For clarity only the a→a and the a→(a+μc) transitions are depicted in Fig. 4 as these are most relevant for the optimization of a-Si:H i-layers for solar cells. The boundaries for vhf (60 MHz) PECVD show two differences compared with those for rf (13.56 MHz) PECVD. First, the a→a roughening transition for the vhf series shifts more gradually to greater thickness with increasing R. As a result, just before the a→(a+μc) transition, the a→a roughening transition occurs at a much larger thickness for the lower rate (0.5 Å/s) rf deposition. Second, in the narrow range 10<R<20, the a→(a+μc) transition thickness is shifted to lower values at the higher (vhf) frequency. This latter difference suggests a much higher density of microcrystallites nucleating from the amorphous phase for vhf compared to rf frequencies. As will be seen shortly, such a strong effect is specific to the growth process on c-Si substrates, and therefore is not particularly device-relevant.

Next we will discuss in greater detail the differences in the a→a roughening transition thickness observed between a-Si:H films prepared by vhf and rf PECVD. Previous extensive correlations have shown that a-Si:H material with the largest a→a transition thickness provides the best performance when incorporated as the i-layer of an a-Si:H-based solar cell. Based on these correlations, two conclusions can be made regarding the comparison of the a→a roughening transition in Fig. 4.

First, similar transition thicknesses for rf and vhf PECVD are obtained at R=0 even though the vhf process provides a factor of ~2.5 higher rate (3.1 Å/s vs. 1.2 Å/s; see Fig. 1). This result suggests that at R=0 the deposition rate of a-Si:H films can be increased without loss of material quality by increasing the plasma frequency from rf (13.56 MHz) to vhf (60 MHz). As R is increased to its optimum value, however, the a→a roughening transition increases much more rapidly for the lower rate rf depositions. In fact at R=10, the a→a roughening transition thickness is > 4000 Å for rf deposition at

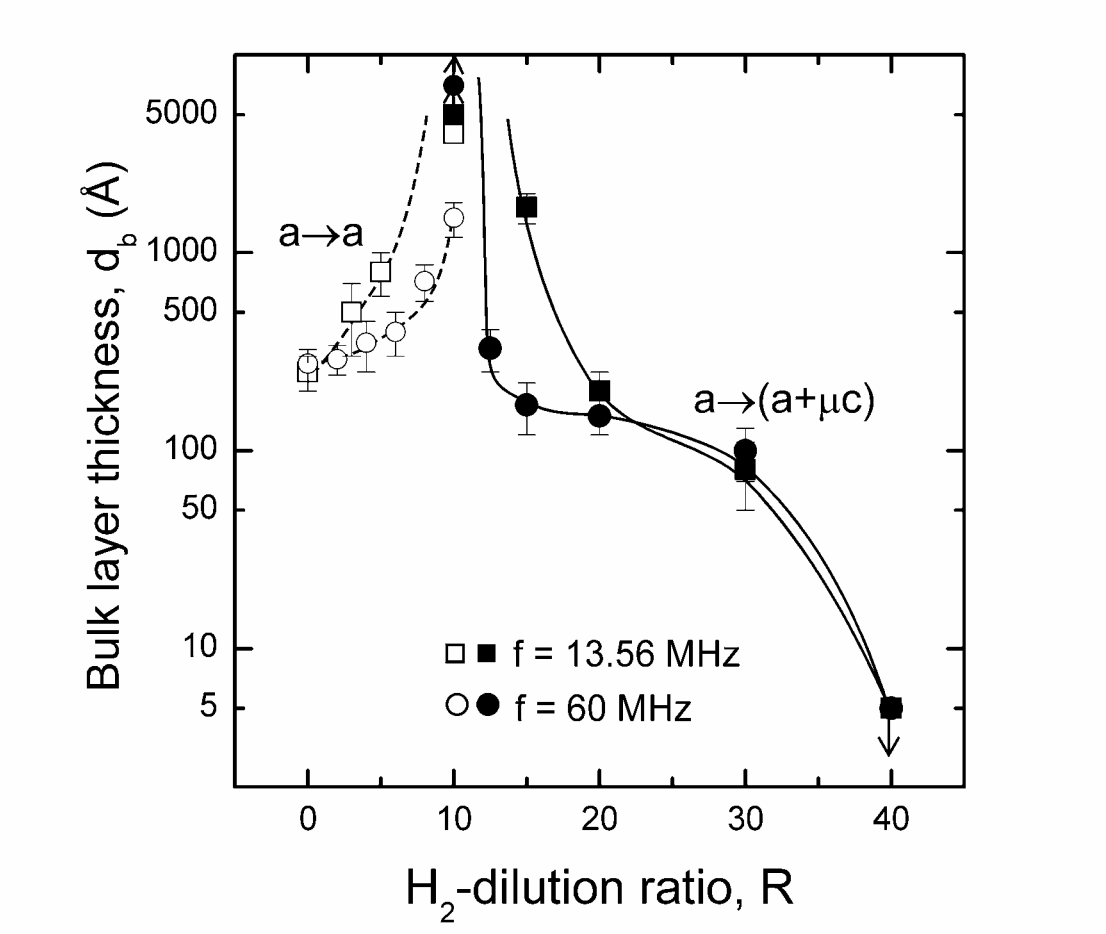

Figure 4: Superimposed phase diagrams for two series of PECVD Si:H films deposited on native oxide-covered c-Si substrates using rf (13.56 MHz) and vhf (60 MHz) plasma frequencies at low power (0.08 mW/cm^2) and low pressure (< 0.5 Torr). The (up, down) arrows indicate that the transition occurs (above, below) the designated value.

0.5 Å/s versus ~1300 Å for vhf deposition at 1.3 Å/s. A comparison of the R=10 vhf (60 MHz) a-Si:H deposition in Fig. 3 with a series of rf (13.56 MHz) depositions performed at elevated rates simply by increasing the plasma power demonstrates that the vhf a-Si:H roughening characteristic is very similar to the rf a-Si:H roughening characteristic for the same deposition rate. This result is shown in Fig. 5, where the surface roughness evolution for the R=10 vhf deposition is superimposed upon the corresponding rf results, the latter data sets obtained at different rates by elevating the plasma power under otherwise identical low pressure conditions.

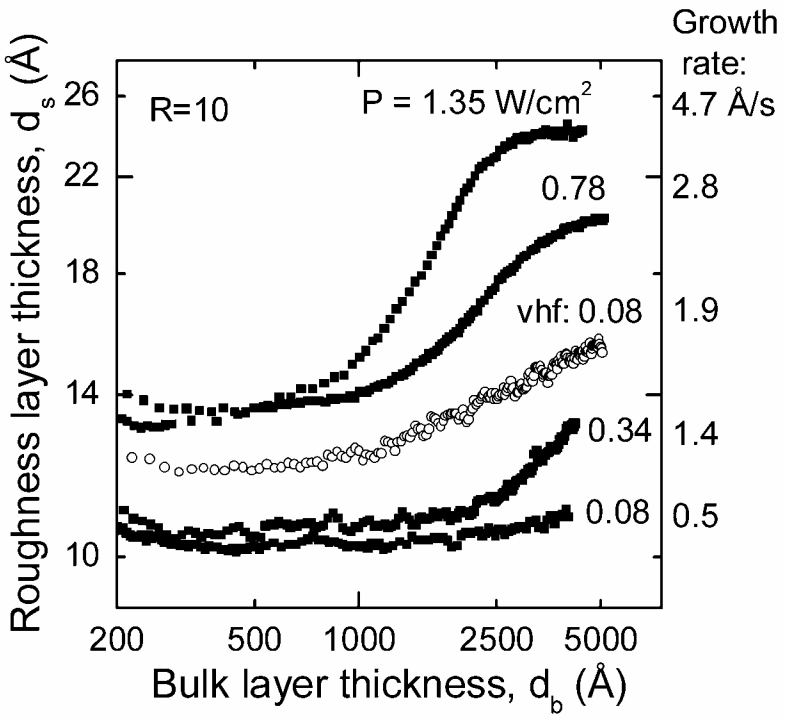

Figure 5: Surface roughness layer thickness versus bulk thickness for a series of R=10 films prepared by rf (13.56 MHz) PECVD at different plasma power levels, and for an R=10 film prepared by vhf (60 MHz) deposition at the lowest plasma power (0.08 W/cm^2). A low total pressure (0.4 Torr) was used throughout.

Finally Fig. 6 shows a comparison of the a→a roughening transition thicknesses for three low pressure processes (i) rf PECVD with minimum plasma power (0.08 W/cm^2, yielding **0.5 Å/s** at R=10); (ii) rf PECVD with high power (0.8 W/cm^2; yielding **3.5 Å/s** at R=10); and (iii) vhf PECVD with minimum power (0.08 W/cm^2, yielding **1.9 Å/s** at R=10). In all cases R=10 lies just below the a→(a+μc) boundary for a thick film. It is clear that the results for vhf PECVD trend from the low power toward the high power rf series with increasing R. Thus, it is clear that the increase in rate without loss of material quality possible with vhf over rf at R=0 is not sustained as R is increase to its optimum value of R=10 just below the a→(a+μc) boundary.

In summary, we are forced to conclude that under the optimum conditions, i.e., for depositions just below the a→(a+μc) boundary, there is no advantage to using vhf over rf deposition, the latter performed at elevated power to ensure the same rates.

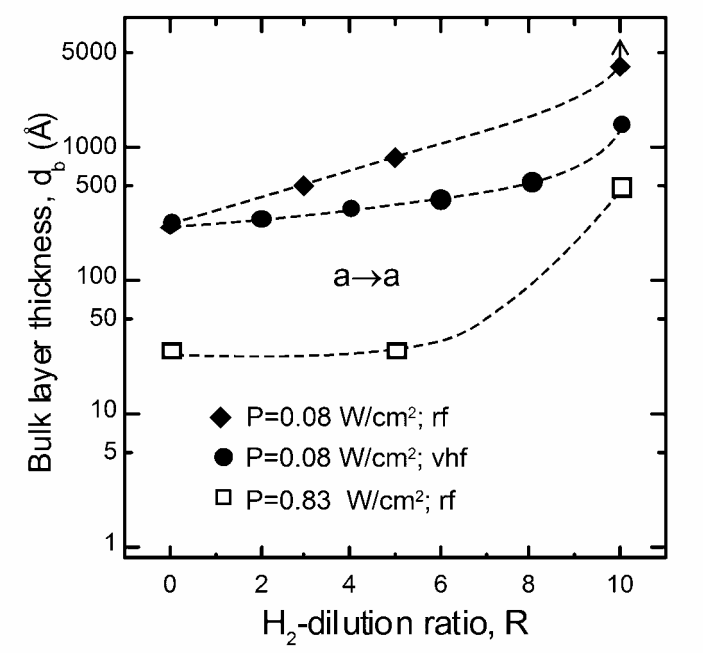

Figure 6: The a→a roughening transition thickness as a function of H_2-dilution ratio for three deposition series at low pressure (<0.5 Torr): (i) rf PECVD with minimum plasma power (0.08 W/cm^2, yielding 1.2 Å/s at R=0 and **0.5 Å/s** at R=10); (ii) rf PECVD with high plasma power (0.8 W/cm^2; yielding 8.0 Å/s at R=0 and **3.5 Å/s** at R=10); and (iii) vhf PECVD with minimum power (0.08 W/cm^2, yielding 3.1 Å /s at R=0 and **1.9 Å/s** at R=10).

Low Power and Pressure Si:H Depositions: R=0 a-Si:H Substrates

Figure 7 shows the microstructural evolution for Si:H films prepared by vhf (60 MHz) PECVD at the minimum plasma power (0.08 W/cm^2) and low pressure (< 0.5 Torr) [process (1)] on underlying R=0 a-Si:H films. These results can be compared with the corresponding ones in Fig. 3 for crystalline Si wafer substrates. This comparison is shown in Fig. 8 where the simple phase diagrams, including only the a→(a+μc) transition thickness, for vhf deposition on the two substrates are superimposed for comparison. As in the case of rf PECVD reported earlier, it is evident that the phase boundary in vhf PECVD shifts to much higher R when R=0 amorphous Si:H substrates are used instead of standard Si wafers. For example, at R=40 the single-phase μc-Si:H nucleates immediately on native-oxide/c-Si, whereas an optimum 200 Å thick interface i-layer can

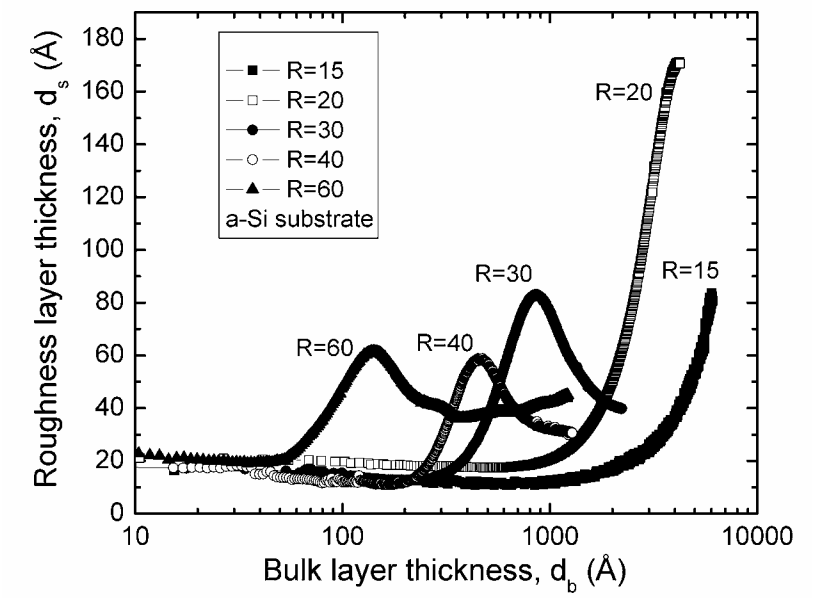

Figure 7: Surface roughness layer thickness (d_s) versus bulk layer thickness (d_b) for deposition of Si:H films by vhf (60.0 MHz) PECVD using H_2-dilution levels of R=15, 20, 30, 40 and 60 at low power (0.08 mW/cm^2) and low pressure (< 0.5 Torr) on R=0 a-Si:H substrates. All films exhibit a→(a+μc) roughening transitions, whereas only the films with R≥30 exhibit clear (a+μc)→μc smoothening transitions (peaks).

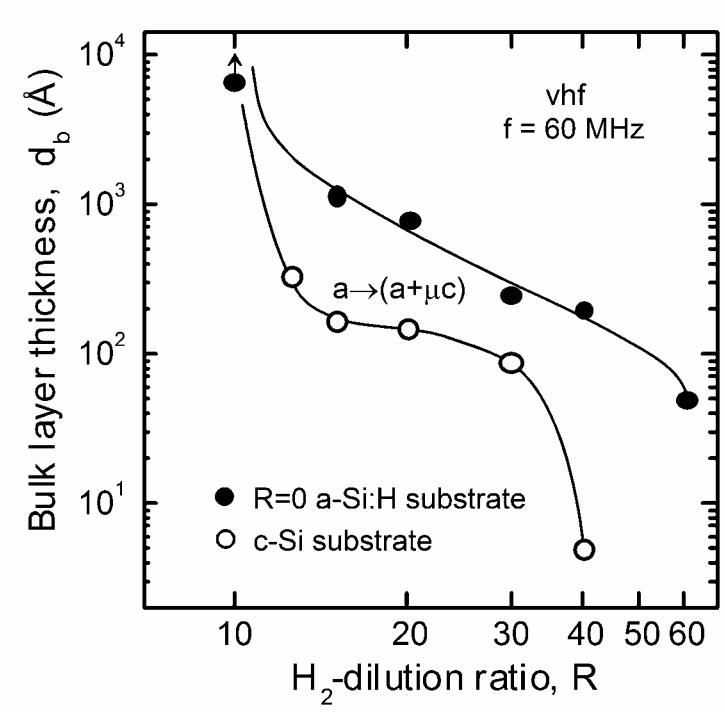

Figure 8: Simple phase diagrams, including only the a→(a+μc) transition thickness, for vhf (60.0 MHz) PECVD of Si:H at low power (0.08 mW/cm^2) and low pressure (< 0.5 Torr) on c-Si wafer substrates (open circles) and R=0 a-Si:H film substrates (filled circles).

be obtained on R=0 a-Si:H (or more importantly, on the p-layer of the p-i-n solar cell). This result shows clearly that the phase of the deposited material is controlled by the substrate in the *protocrystalline* Si:H growth regime.

A comparison of phase diagrams for rf and vhf PECVD both prepared on the R=0 a-Si:H substrate films is shown in Fig. 9. In this figure, the results for vhf (60 MHz) PECVD are depicted as the circles and the results for rf (13.56 MHz) PECVD by the squares. Overall, the thicknesses of the a→(a+μc) and (a+μc)→μc transitions for the two different frequencies are in close agreement. The only significant difference in Fig. 9

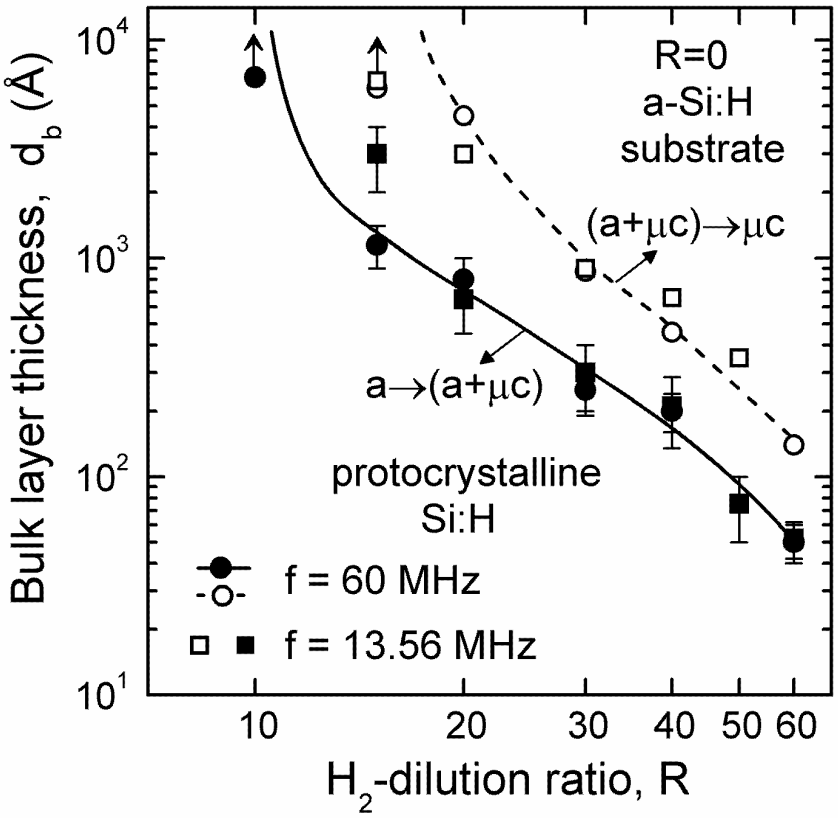

Figure 9: Superimposed phase diagrams comparing Si:H depositions using rf (13.56 MHz; squares) and vhf (60 MHz; circles) plasma excitation on R=0 a-Si:H substrate films. The filled and open points denote the a→(a+μc) and (a+μc)→μc transitions, respectively. Both series of depositions were performed at low plasma power (0.08 mW/cm^2) and pressure (< 0.5 Torr) under otherwise identical conditions.

occurs with R=15 in which case the a→(a+μc) transition is shifted to lower thickness for the vhf deposition, an effect similar to that observed in Fig. 4, but not as strong. This effect may suggest that the stress in the vhf PECVD films builds up more rapidly with thickness than that in the rf films, however the origin of this behavior is unclear.

Perhaps the most important consequence of the close similarities of the results in Fig. 9 is that the two-step optimization procedure developed for the rf PECVD i-layers of a-Si:H p-i-n and n-i-p cells would apply equally well for vhf PECVD i-layers.

Comparison of vhf and rf PECVD of a-Si:H at High Pressure: ~ 3.3 Å/s

It is generally recognized that although the highest quality materials can be prepared by rf PECVD at very low rates (0.5 Å/s) by combining the lowest possible power with low gas pressure (<0.5 Torr), this process fails to provide high quality materials at higher rate simply by elevating the plasma power. At the lowest power, any ion bombardment may exert a beneficial influence by promoting dehydrogenation reactions within the top monolayer of the growing surface. At higher power levels, energetic bombardment is likely to cause damage to the near-surface region of the film below the topmost monolayer which is then frozen in as the film accumulates. A straightforward approach to eliminate this damage is to operate the deposition at higher pressures. Operation of the plasma at higher pressures is also known to shift the a→(a+μc) transition to high R values presumably due to the depletion of atomic H from the plasma via reaction with SiH_4.

Figure 10 shows the deposition rate as a function of R for rf and vhf PECVD of Si:H under conditions of elevated power (rf: 0.34 W/cm^2; vhf: 0.53 W/cm^2) and high pressure (fixed at 4 Torr), leading to moderate deposition rates (~3.3 Å/s) just below the a→(a+μc) boundary for a thick film [process (2), above]. Results are shown for rf PECVD with R spanning from 10 to 80, and for vhf PECVD with R spanning a narrower

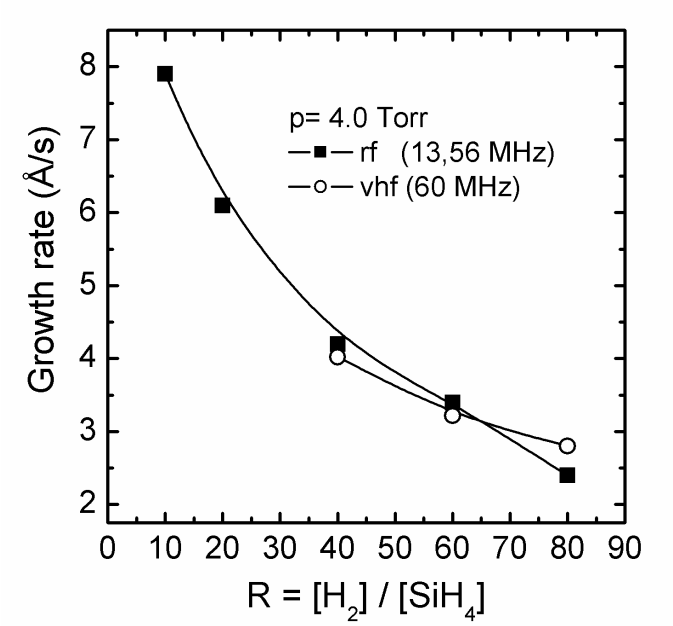

Figure 10: Deposition rate versus H_2-dilution ratio R for Si:H film growth by rf (13.56 Hz) and vhf (60.0 MHz) PECVD under elevated power and high pressure (p = 4.0 Torr) conditions that yield moderate deposition rates (~3.3 Å/s) just below the a → (a+μc) transition (R=60).

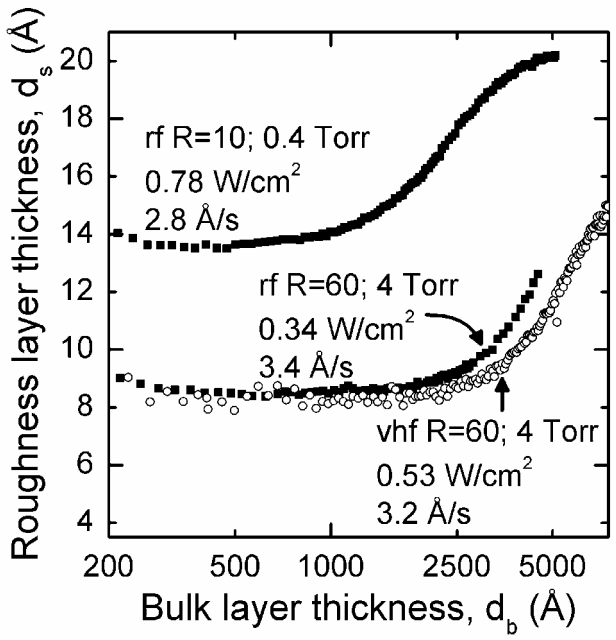

Figure 11: Surface roughness layer thickness versus bulk layer thickness for films prepared by rf (13.56 MHz) PECVD at low pressure (0.4 Torr) and by rf and vhf (60 MHz) PECVD at high pressure (4 Torr). R was maximized while ensuring a-Si:H deposition throughout the thickness, and the power density was selected for similar rates (2.8 - 3.4 Å/s).

range from 40 to 80, since vhf PECVD at 4 Torr exhibited a narrower range of plasma stability. Figure 11 shows the microstructural evolution of three Si:H films prepared at moderates rates (2.8-3.4 Å/s) just below the a→(a+μc) transition for a thick layer. The two moderate rate a-Si:H films that exhibit the largest a→a roughening transition thickness, ~ 3000 Å, and hence the highest quality, are those prepared under high pressure conditions (4 Torr), including both rf and vhf depositions. In contrast, the film with the poorer surface stability with an a→a transition of ~1500 Å -- in spite of the fact that its rate is somewhat lower than those of the high pressure depositions -- is the one prepared under low pressure conditions (0.4 Torr) by rf PECVD. The lower rate may be a factor in this case (and thus the ~1500 Å transition is an optimistic upper limit) since the a→a roughening transition shifts rapidly to lower thickness with increasing rate under low pressure conditions (see Fig. 12). The apparent small improvement in vhf vs. rf for the two high pressure depositions may also be attributed at least in part to its lower rate.

Figure 12 summarizes the conclusions associated with Fig. 11 through a depiction of phase diagrams for low pressure and high pressure depositions that lead to 3.2-3.5 Å/s rates at an R value just below the a→(a+μc) transition for a thick layer. Most of the results here are from rf depositions presented in earlier reports. The poor plasma stability at 4 Torr for vhf PECVD has prevented the collection of an extensive data set in this case. However, the available data (triangles) suggest similar results for both rf and vhf at high pressures and at optimized R values just below the a→(a+μc) transition for a thick layer (R=60). Thus, in the depositions performed thus far, including those at low rates and low pressures as well as moderate rates and high pressures, *there is no significant advantage in adopting vhf PECVD over rf PECVD when optimum R values are employed for both.*

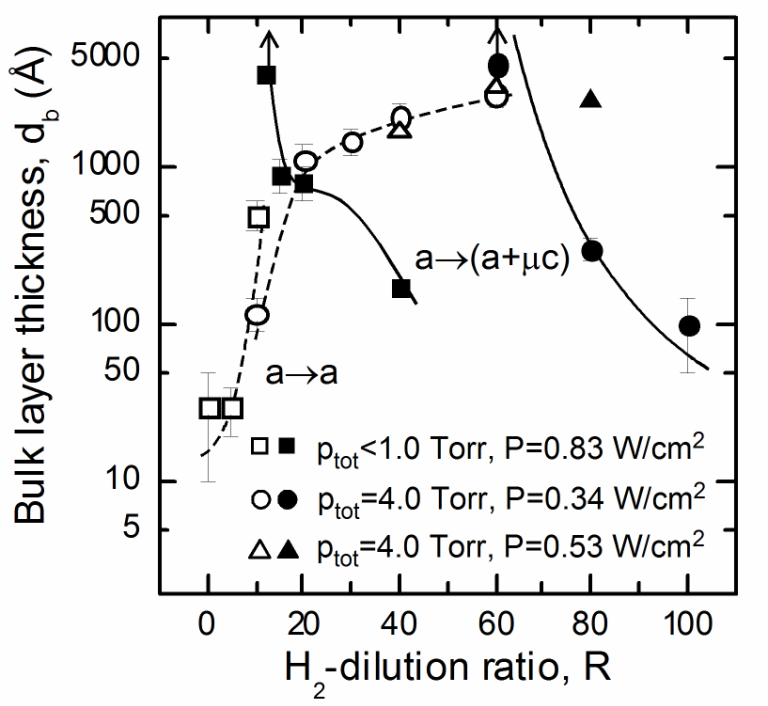

Figure 12: Phase diagrams for Si:H film depositions on c-Si substrates at 200°C by rf (13.56 MHz) PECVD under elevated power conditions using low and high total gas pressures, including (P=0.83 W/cm^2, p_{tot}<0.5 Torr) (squares), and (P=0.34 W/cm^2, p_{tot}=4.0 Torr) (circles). The open symbols and broken lines indicate a→a transitions and the closed symbols and solid lines indicate a→(a+μc) transitions. The points indicated by **triangles** represent results obtained by **vhf** (60 MHz) **PECVD** under elevated power and high pressure conditions (P=0.53 W/cm^2, p_{tot}=4.0 Torr) over a narrower range of R where the plasma is stable. The up arrows indicate that the transition occurs above the identified thickness values.

Comparison of vhf and rf PECVD of a-Si:H at High Pressure: ~ 6.5 Å/s

In order to explore further the final conclusion of the previous section, we employ rf and vhf conditions that (i) yield essentially identical deposition rates just below the a→(a+μc) transition for a thick film and (ii) provide higher vhf plasma stability, in particular lower pressure conditions. Thus, a third comparison of rf and vhf depositions was performed in which the deposition rate was fixed at 6.5 Å/s just below the a→(a+μc) transition for a thick film.

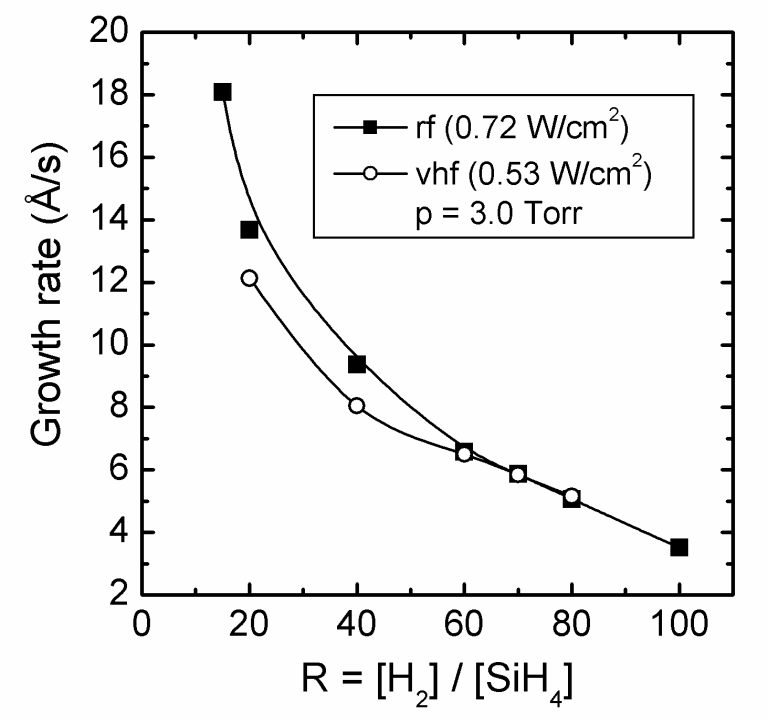

Figure 13: Comparison of the deposition rates for vhf (60 MHz) and rf (13.56 MHz) Si:H film growth as a function of R at elevated power and a high pressure of 3 Torr. Power levels are chosen to yield similarly high deposition rates (~6.5 Å/s) just below the a → (a+μc) transition (R=60).

Figure 13 shows the deposition rates as a function of the H_2-dilution ratio for rf and vhf depositions at high pressure (3 Torr) and elevated power levels (rf: 0.72 W/cm^2; vhf: 0.53 W/cm^2) selected for a deposition rate of 6.5 Å/s just below the a→(a+μc) transition for a thick film [process (3), above].

Figure 14 shows the microstructural evolution, specifically the surface roughness layer thickness (d_s) versus the bulk layer thickness (d_b) for the growth of rf (13.56 MHz) PECVD Si:H films that remain amorphous throughout the bulk thickness evolution. These films were prepared using different hydrogen dilution levels (R=15, 20, 40, and 60) at high power (0.72 W/cm^2) and pressure (3 Torr) on native oxide-covered c-Si substrates. As shown in Fig. 13, the deposition rates for these films range from 18 Å/s

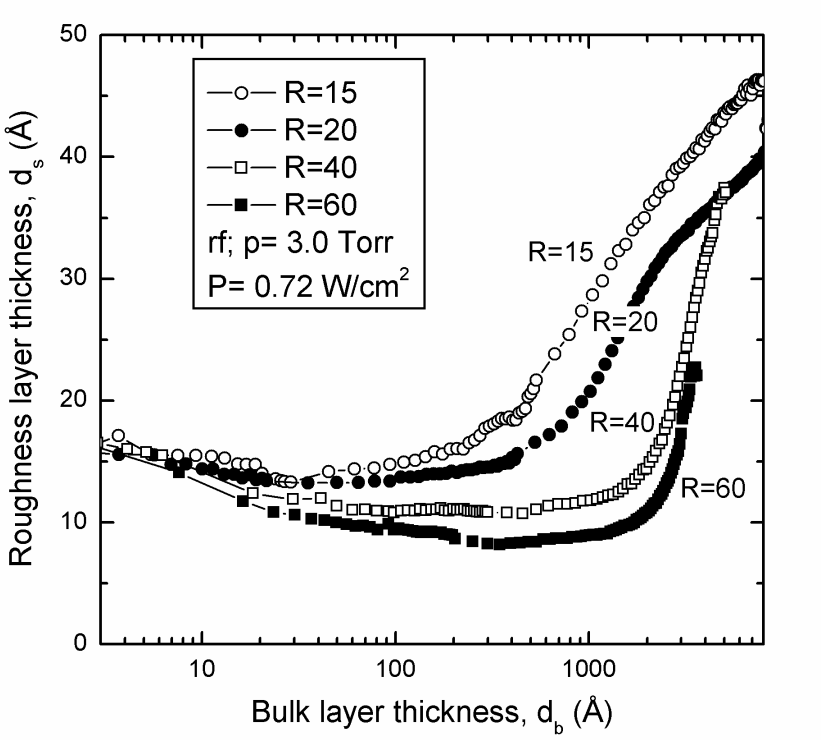

Figure 14: Surface roughness layer thickness (d_s) versus bulk layer thickness (d_b) for deposition of a-Si:H films by rf PECVD using H_2-dilution levels of R=15, 20, 40, and 60 at a plasma power of 0.72 W/cm^2 and a total pressure of 3.0 Torr on (native oxide)/c-Si substrates.

at R=15 to 6.5 Å/s for R=60, just below the a→(a+μc) transition. In this figure, the three manifestations of improved material quality are clearly evident with increasing R:

(i) increased surface smoothening (both rates and amplitudes) associated with the coalescence of initial nuclei in the first 100 Å of deposition;

(ii) reduced surface roughness layer thickness at the stable surface value; and

(iii) increased thickness of the a→a roughening transition.

Figure 15 shows the microstructural evolution of rf PECVD Si:H films deposited using H_2-dilution levels of R= 70, 80, and 100 under other identical conditions as those in Fig. 14. Each of these films crosses the a→(a+μc) transition during the growth, at a transition thickness that decreases with increasing R. Only the deposition with R=100 also crosses the (a+μc)→μc transition during growth, at a thickness of ~700 Å in this case.

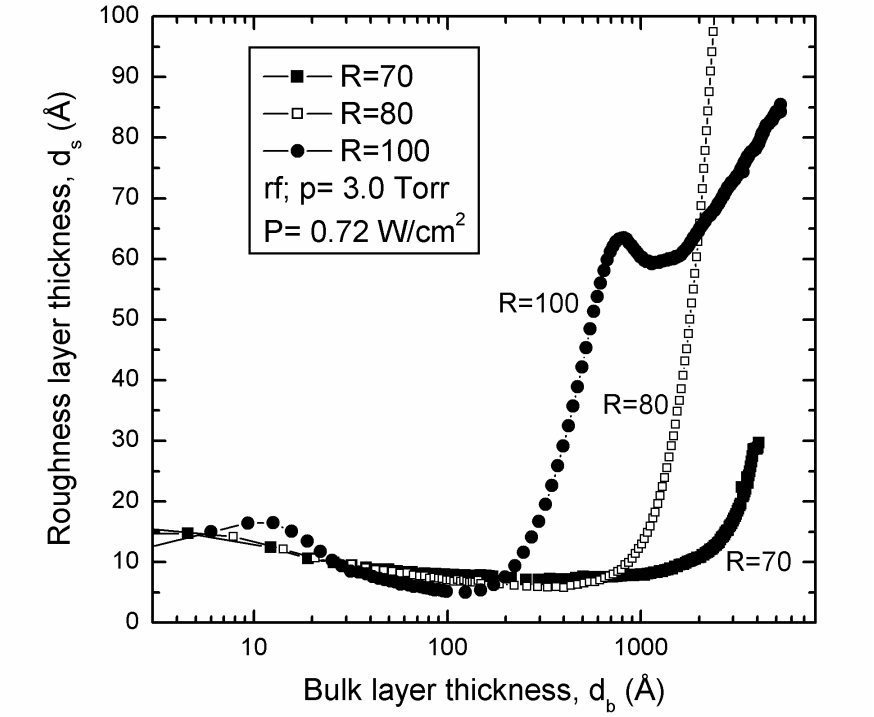

Figure 15: Surface roughness layer thickness (d_s) versus bulk layer thickness (d_b) for deposition of Si:H films by rf PECVD using H_2-dilution levels of R=70, 80, and 100 at a power level of 0.72 W/cm^2 and a total pressure of 3.0 Torr on (native oxide)/c-Si substrates.

The combined results are summarized in Fig. 16 for the microstructural evolution during Si:H film growth by vhf PECVD using H_2-dilution ratios R=20, 40, 60, 70, and 80 at elevated plasma power (0.53 W/cm^2) and 3 Torr pressure. In this case, similar trends occur as in the case of rf, but in Fig. 16 it is important to distinguish the a$\rightarrow$a roughening transitions that occur for R$\leq$60 from the a$\rightarrow$(a+μc) transitions that occur for R$\geq$70. As usual, this can be done on the basis of the optical functions which are deduced for the Si:H film at the end of the deposition.

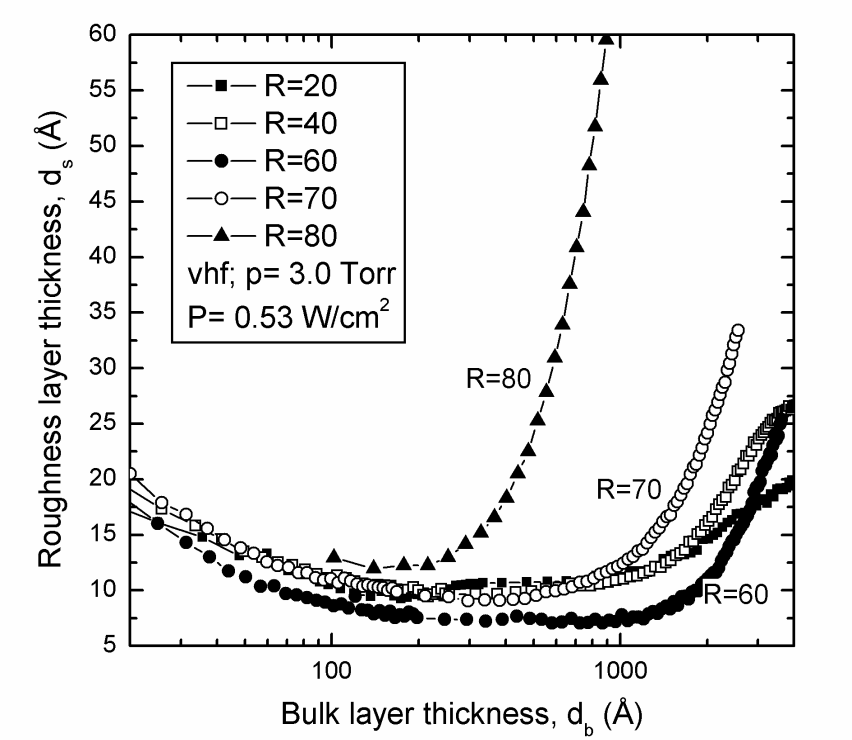

Figure 16: Surface roughness layer thickness (d_s) versus bulk layer thickness (d_b) for vhf (60 MHz) PECVD of Si:H films using H_2-dilution levels of R=20, 40, 60, 70, and 80 at a power level of 0.53 W/cm^2 and a total pressure of 3.0 Torr on (native oxide)/c-Si substrates.

Figure 17 shows the superimposed phase diagrams comparing the rf (13.56 MHz) and vhf (60 MHz) processes that yield identical deposition rates of 6.5 Å/s at R=60 just below the a→(a+μc) transition (see Fig. 13). The key conclusion of these two sets of depositions is the observation that both rf and vhf PECVD a-Si:H films exhibit identical a→a roughening transition thicknesses at the optimum R value of 60 just before the a→(a+μc) transition. On the basis of this observation, we can conclude that both R=60 depositions exhibit similar material quality, and that vhf PECVD provides no significant advantage over rf PECVD when high rate deposition conditions are optimized and

identical deposition rates are compared. In addition to this key conclusion, additional characteristics are evident in Fig. 17 that are consistent with previous observations. First,

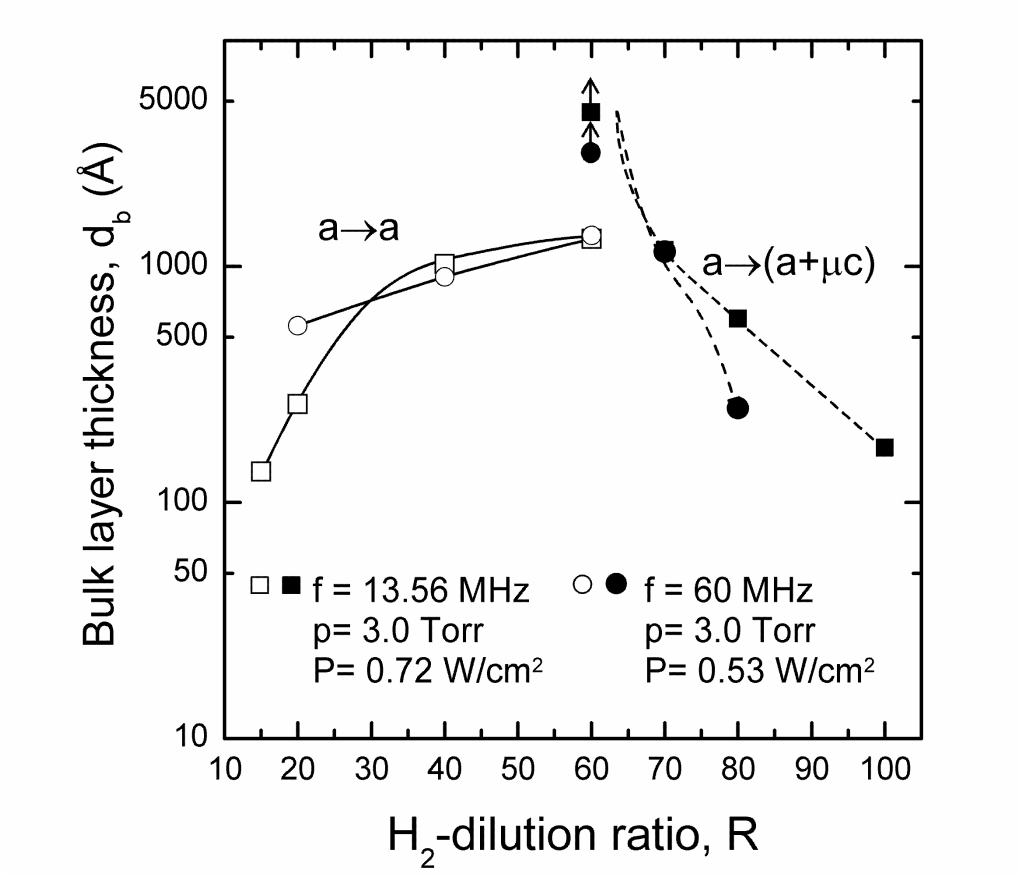

Figure 17: Superimposed phase diagrams for two series of PECVD Si:H films deposited on native oxide-covered c-Si substrates using plasma frequencies of 13.56 and 60 MHz, at elevated plasma power levels of 0.72 W/cm^2 (rf) and 0.53 W/cm^2 (vhf) and at 3 Torr total pressure.

at the lowest value of R (R=20) accessible to vhf PECVD, the a→a roughening transition thickness for vhf deposition is significantly higher than that for rf deposition, suggesting that under non-optimal conditions, in particular insufficient H_2-dilution level, the vhf process does provide an improvement over the corresponding rf process. This conclusion was also reached in consideration of the low power, low pressure rf-vhf deposition comparison. Second, at the highest value of R (R=80) accessible to vhf PECVD, the

a→(a+μc) occurs at a lower thickness for vhf PECVD than for rf suggesting a more rapid development of stress-induced crystallinity. Although such observations were noted earlier in comparing vhf and rf processes at low power and low pressure, the differences were not found to be of significance for devices. In particular when R=0 a-Si:H substrates are used, such differences tend to be suppressed or eliminated.

Finally, it is of interest to compare the deposition phase diagrams for the two rf deposition processes at high pressure, one yielding a rate of 3.4 Å/s just before the a→(a+μc) transition, and the other yielding a rate of 6.5 Å/s under the corresponding conditions. These results are shown in Fig. 18 wherein the lower rate is obtained with power and pressure values of 0.34 W/cm^2 and 4 Torr and the higher rate is obtained with corresponding values of 0.72 W/cm^2 and 3 Torr. Two key observations are evident here that are consistent with many previous investigations. First and most importantly, the entire a→a roughening transition thickness is shifted to decreasing thickness at the higher rate, a trend that clearly reveals degrading material properties with increasing deposition rates. However, the a→a roughening transition thickness just below the a→(a+μc) boundary remains above 1000 Å, which is still a factor of two higher than that observed under the low pressure deposition conditions with almost a factor of two lower rate. As a result, we suggest that the high power, high pressure conditions may give rise to reasonable device performance at rates > 6 Å/s, without resorting to unconventional deposition methods.

In future work, these strategies in rf PECVD will be applied in the fabrication of p-i-n and n-i-p solar cell devices with i-layers prepared first at 3 Å/s and then at 6 Å/s. In addition, the strategies will be considered for possible application in higher rate amorphous silicon-germanium deposition. Currently, we are setting up the gas lines for the fabrication of these alloys.

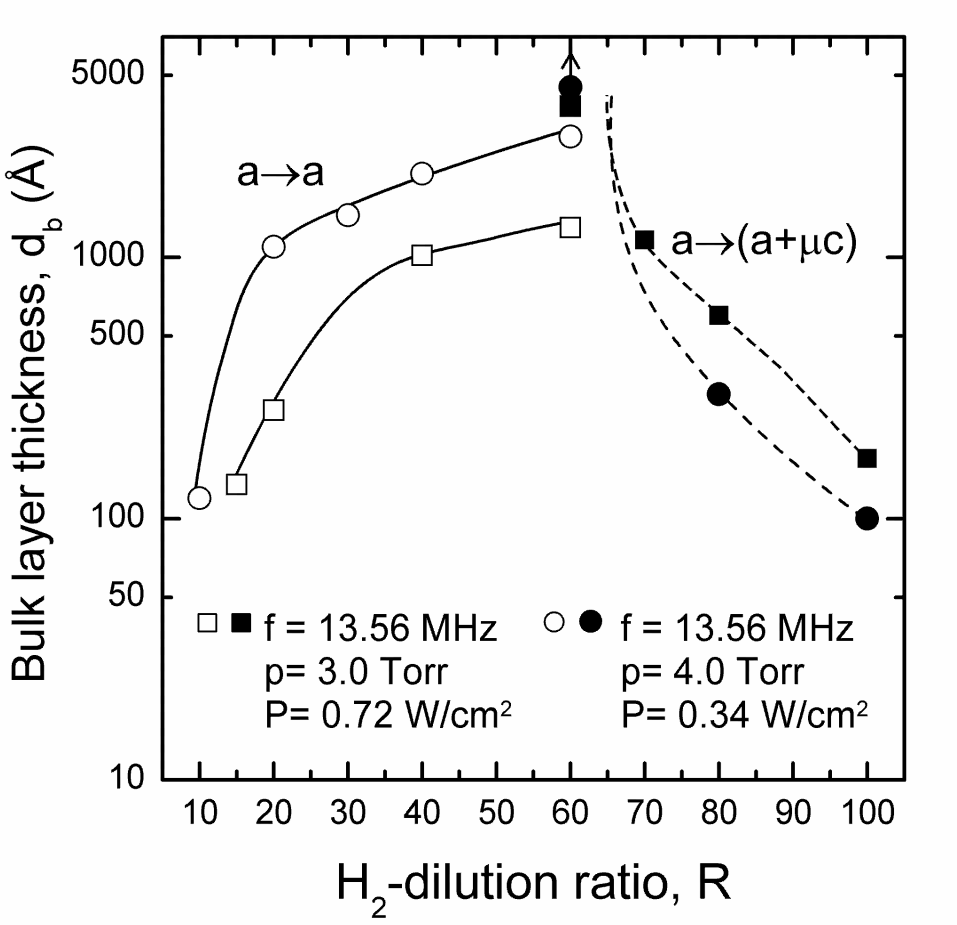

Figure 18: Superimposed phase diagrams for two series of PECVD Si:H films deposited on native oxide-covered c-Si substrates. Both series apply rf plasma excitation (13.56 MHz) under high pressure conditions, one with a power level of 0.34 W/cm^2, yielding a rate of 3.4 Å/s just before the a→(α+μc) transition and the other with a power level of 0.72 W/cm^2, yielding a rate of 6.5 Å/s just before the a→(a+μc) transition.

Report Including: Task 3 Device loss mechanisms

Studies were continued during this quarter on identifying, separating and quantifying carrier recombination in the bulk and at the p/i interfaces of a-Si:H solar cells. It has been shown in an earlier report[2] that the distributions of defects across the i-layers are homogeneous. Thus, there is no evidence of the large densities of defects at the p/i or n/i interface regions predicted by the defect pool model. These conclusions were established from our results on J_D-V characteristics of cell structures having different p/i interface regions and from the observed thickness dependence of the J_D-V characteristics of the cells with controlled p/i interface recombination. In order to further quantify the p/i recombination and to establish the range of voltages in the J_D-V characteristics over which bulk recombination dominates, studies were carried out on J_D-V characteristics of cells having R=0 and R=10 intrinsic layers with different thicknesses. It is found that, even in cells in which the p/i interface regions have not been fully optimized, their J_D-V characteristics still exhibit a thickness dependence over a wide range of voltage.

This thickness dependence is illustrated in Figure 19 where the results on J_D-V characteristics are shown for two p-i-n cells with 0.4μm and 0.8μm R=10 "straight" i-layers, in which the p/i interface regions have not been modified, e.g., by introducing 200Å of a-Si:H having different R. In the results shown, the two cells have identical p/i interface regions, which then yield the same p/i interface recombination, whereas the bulk recombination is controlled by the change in the thickness of the i-layer. From such results it is possible first to separate and then to evaluate the contributions at the p/i

[2] NREL Annual Report 2002, Penn State Univ.

interfaces and those of the bulk, the latter being proportional to the i-layer thickness. As a consequence it is possible to extract the J_D-V characteristic expected for a cell structure in which the p/i interface contribution to carrier recombination is negligible compared to that of the bulk. This is obtained from the results in Figure 19 by directly subtracting the J_D-V characteristic of the cell with 0.4μm i-layer from that of the cell with 0.8μm i-layer. In this way the recombination at the p/i interface is cancelled out. The resulting J_D-V characteristics thus corresponds to that of a cell structure having an i-layer thickness of 0.8 – 0.4 = 0.4μm with negligible recombination at the p/i interface region.

Such a J_D-V characteristic is shown in Figure 20 along with the experimental results obtained for a p-i-n cell with a 0.4μm R=10 bulk i-layer and a 200Å R=40 i-layer at the p/i interface. Also included in this figure are the characteristics of the cells in Figure 19. It can be seen in Figure 20 that there is excellent overlap between the J_D-V characteristic extracted from the results in Figure 19 and that of the cell structure in which the p/i interface recombination has been reduced with an R=40 p/i interface region. There is a clear indication that p/i interface recombination can be virtually eliminated by the insertion of a high band gap, high quality protocrystalline material (such as that obtained with R=40) at the p/i interface. It can be seen in Figure 20 that divergence between the J_D-V characteristics of the cells with and without p/i interface layer occurs around 0.55V at which point the contributions of the p/i interface recombination of the non-optimized cell structure begin to apprear. For voltages smaller than this, the p/i interface contributions are negligible compared to the recombination in the bulk. It is important to point out here that at the higher voltages even though the p/i interface recombination becomes more and more significant it can be still smaller than that of the

bulk over extended regions of voltage. In fact, it can be seen in Figure 20 that the thickness dependence of the J_D-V characteristics is still present at the higher voltages, even up to the values of open circuit voltage (~0.89 V) under 1 sun illumination. This bulk contribution is reflected in the thickness dependence of the values of 1-sun V_{OC} for the cells in Figure 19, which exhibit a difference of about 15 mV. The results on the thickness dependence obtained here show that even in the R=10 "straight" cells without the R=40 p/i interface layer, the recombination currents are not determined solely by p/i interface recombination even at the high voltages corresponding to 1-sun V_{OC} values. This allows the light induced changes in these V_{OC}'s to be used in probing the gap states limiting V_{OC}.

Results were also obtained for R=0 "straight" cells with 0.4μm and 0.8μm thick i-layers as shown in Figure 21. Again excellent agreement is obtained between the characteristic corrected for p/i interface recombination and that of the cell with a R=40 p/i interface region. It can be seen in the figure that the presence of the R=40 layer at the p/i interface again eliminates contributions to the J_D-V characteristics due to recombination there. For the results on the R=0 cells, with and without the R=40 p/i interface region, the divergence between their J_D-V characteristics now occurs at around 0.35 V, a value smaller than that for the R=10 cells in Figure 20 (0.55 V). This reflects the higher p/i interface recombination in the R=0 straight cells than in the R=10 straight cell as would be expected from the lower band gap as well as the absence of protocrystallinity in the R=0 i-layers. That this is indeed the case is reflected in the virtual absence of any thickness dependence in 1 sun V_{OC}'s.

It has been established in this quarter that in both R=10 and R=0 a-Si:H cells, in which the recombination at the p/i interfaces has been reduced by having R=40 interface layers there, the J_D-V characteristics are dominated by bulk recombination over a wide voltage regime. Consequently, differences in the gap states in the R=10 and R=0 intrinsic layers of solar cells can be evaluated directly from their J_D-V characteristics, and correlations can be made between the various resulting parameters and characteristics with those obtained on the corresponding intrinsic films. A detailed study of light induced changes in the J_D-V characteristics of cells with R=0, R=10 intrinsic layers have been undertaken using this novel probe. It appears particularly useful for characterizing the differences in light induced defects that are clearly revealed by the results on the corresponding thin films[3].

[3] J. M. Pearce, J. Deng, R. W. Collins, and C. R. Wronski, "Light Induced Defect States in Hydrogenated Amorphous Silicon Centered Around 1.05 and 1.2eV from the Conduction Band Edge", *Applied Physics Letters*, **83** (18), pp. 3725-3727, 2003.

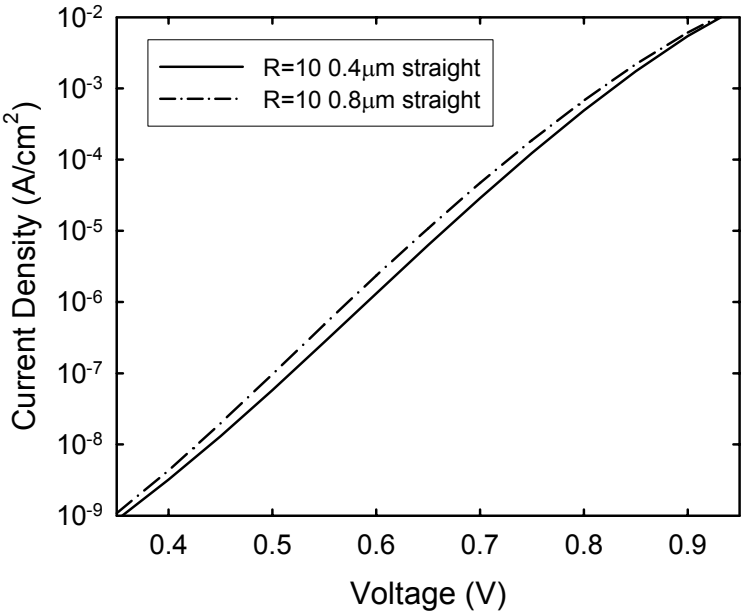

Figure 19: J_D-V characteristics for R=10 a-Si:H cells with two different thickness i-layers.

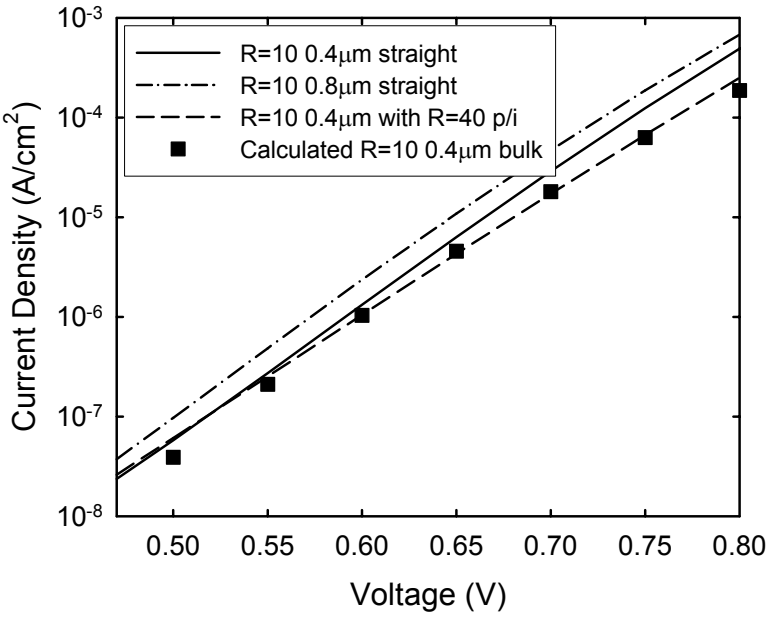

Figure 20: J_D-V characteristics for R=10 cells with and without a p/i interface layer and the predicted result for a R=10 cell structure in which the p/i recombination is negligible.

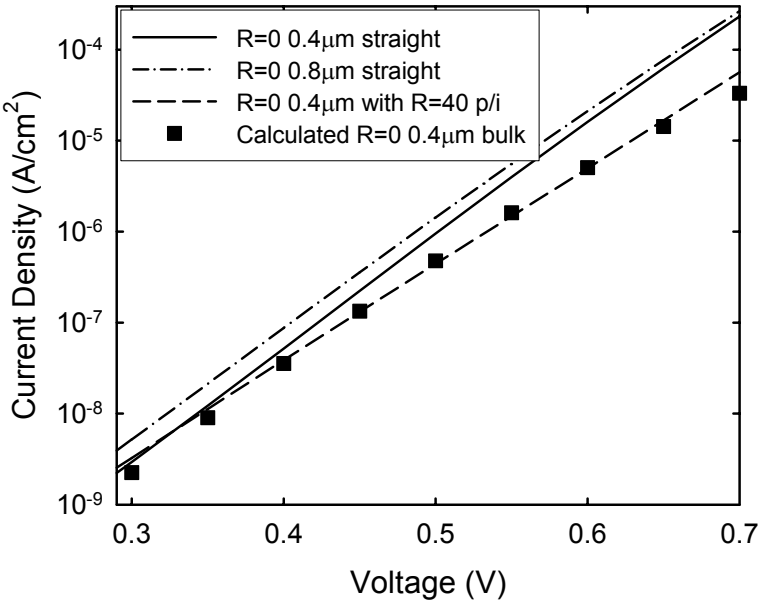

Figure 21: J_D-V characteristics for R=0 cells with and without a p/i interface layer and the predicted result for a R=0 cell structure in which the p/i recombination is negligible.